Supplementary Information

S1 Microstructural characterization

The phase composition of the samples was identified by X-ray diffraction apparatus (D8 ADVANCE, Bruker, Germany) using CuKα radiation from 5° to 90° at a rate of 5°/min. The surface chemical functional groups were recorded with a Nexus 410 spectrometer (Nexus 410, Nicolet, USA) and scanned in the wavelength range of 4000–400 /cm. The microstructural morphology of PDA-Fe_3O_4-Ag nanocomposites was observed by field emission scanning electron microscopy (JSM-7600 F, JEOL Ltd., Japan) and Tecnai 12 transmission electron microscope (Tecnai 12, Philips, The Netherlands). The chemical composition and electronic structure of PDA-Fe_3O_4-Ag before and after MB adsorption were explored from X-ray photoelectron spectroscopy (XPS, Thermo Fisher Scientific K-Alpha, USA) with Al Kα X-rays (hv=1486.68 eV). The 50 eV pass energy and 0.05 eV energy step size were utilised. The vacuum degree of the analysis chamber was 5×10^{-10} Pa, the working voltage was 15 kV, the filament current was10 mA, and the signal accumulation was carried out for 5–10 cycles. The charge correction was performed with the binding energy of C 1s=284.80 eV as the energy standard. The absorbance of dye wastewater solution was determined by UV–vis spectrophotometer (TU-1901, Persee, China) in the range of 190 nm to 900 nm. The maximum absorption wavelengths of CR, MB, MO, NR, RhB, MG and JGB were selected at 498, 660, 465, 450, 550, 617 and 395 nm.

S2 Adsorption kinetics

Adsorption kinetics models generally includes the pseudo-first-order model, the pseudo-second-order model and the intraparticle diffusion model (Wang et al., 2021). The expressions of the three models can be showed as Eqs. (S1), (S2) and (S3) below (Li et al., 2021a):

the pseudo-first-order model equation:

$$\ln(q_e - q_t) = \ln q_e - k_1 t \ , \qquad \text{(S1)}$$

the pseudo-second-order model equation:

$$t/q_t = 1/(k_2 q_e^2) + t/q_e \ , \qquad \text{(S2)}$$

the intraparticle diffusion model:

$$q_t = \mathrm{k_S} t^{\frac{1}{2}} \ , \qquad \text{(S3)}$$

where, q_e (mg/g) is the adsorption capacity at adsorption equilibrium; q_t (mg/g) is the adsorption capacity at time t; k_1 (g/mg/min) is the rate constant of adsorption for pseudo-first-order model; k_2 (g/mg/min) is the rate constant of adsorption for pseudo-second-order model; k_s (g/mg/min$^{0.5}$) is the rate constant of adsorption for intra-particle diffusion model.

S3 Adsorption thermodynamics

The changes of adsorption free energy (ΔG^0, kJ/mol), enthalpy (ΔH^0, kJ/mol) and entropy (ΔS^0, kJ/mol/K) were calculated (Alamin et al., 2021). The relevant expressions can be showed as Eqs. (S4), (S5) and (S6) below (Banisheykholeslami et al., 2021):

$$\Delta G^0 = -\mathrm{R}T \ln \mathrm{K}_0 \ , \qquad \text{(S4)}$$

$$\ln \mathrm{K}_0 = \Delta S^0 / \mathrm{R} - \Delta H^0 / (\mathrm{R}T) \ , \qquad \text{(S5)}$$

$$\Delta H^0 = \Delta G^0 - T\Delta S^0 \ , \qquad \text{(S6)}$$

where, R (8.314 J/mol/K) is the universal constant of gas; K_0 is the equilibrium constant; T (K) is the absolute temperature.

To determine the interactive behavior between the adsorbent and the adsorbate, we tested adsorption isotherm models, including the Langmuir and Freundlich models (Giannakoudakis et al., 2021). Langmuir adsorption isotherm model for monolayer adsorption and Freundlich adsorption isotherm model for multilayer adsorption. The expressions of the two models can be showed as Eqs. (S7) and (S8) below (Zhang et al., 2021):

Langmuir adsorption isotherm equation:

$$1/q_e = 1/q_m + 1/q_m \mathrm{K_L} C_e \ , \qquad \text{(S7)}$$

Freundlich adsorption isotherm equation:

$$\ln q_e = \ln \mathrm{K_F} + 1/\mathrm{n} \ln Ce \ , \qquad \text{(S8)}$$

where, q_e (mg/g) is the adsorption capacity at adsorption equilibrium; q_m (mg/g) is the maximum saturated adsorption capacity; K_L is the adsorption equilibrium constant for Langmuir adsorption isotherm; C_e (mg/L) is the concentration of adsorbate solution at adsorption equilibrium; K_F (L/g) and n are adsorption equilibrium constants for Freundlich adsorption isotherm, representing adsorption capacity and adsorption density in adsorption, respectively.

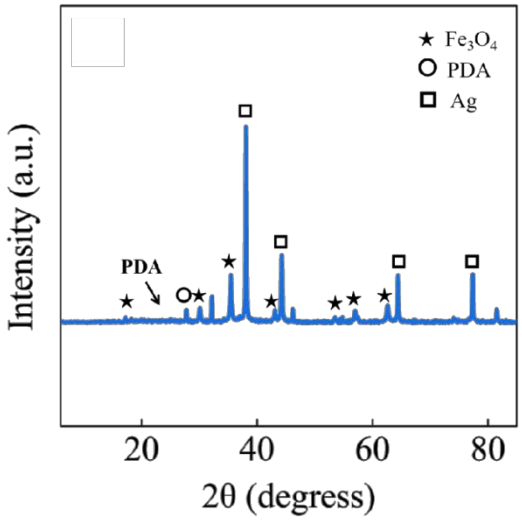

Fig. S1 The XRD pattern of PDA-Fe_3O_4-Ag.

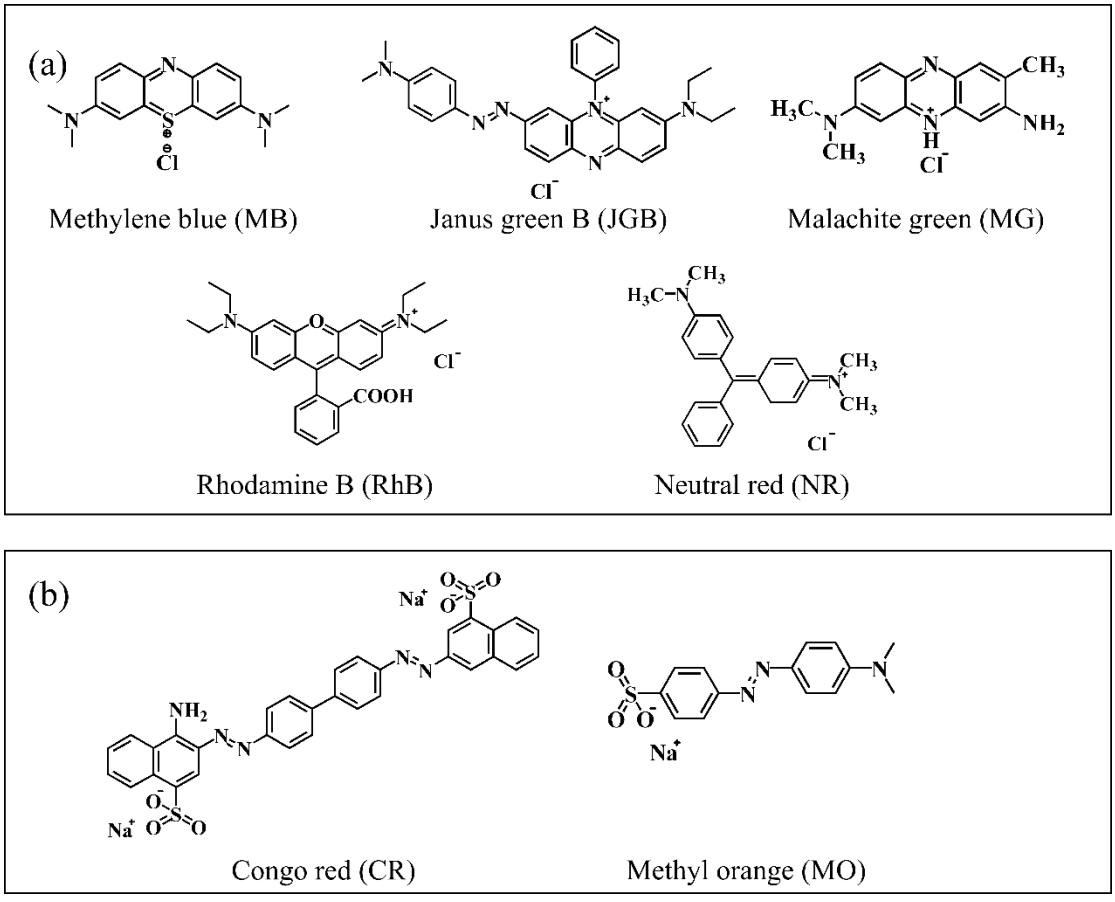

Fig. S2 The structural formulas for various dyes: (a) Cationic dyes; (b) Anionic dyes.

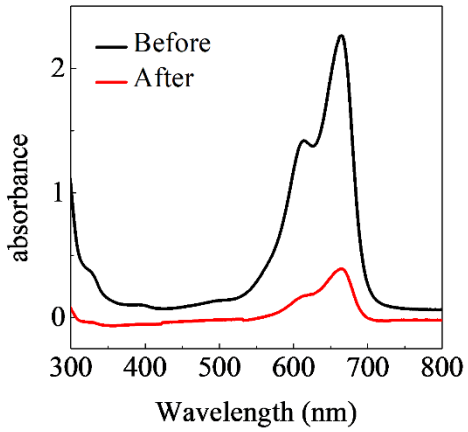

Fig. S3 The UV spectrum of MB before and after adsorption.

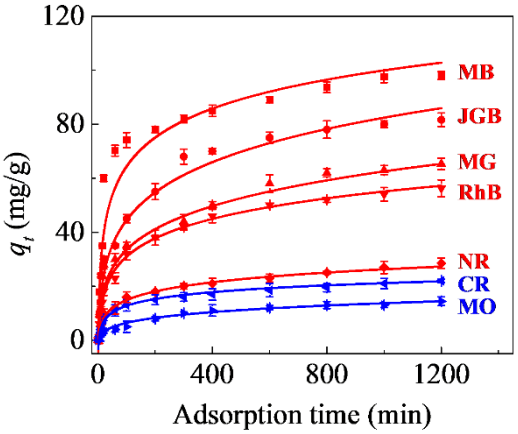

Fig. S4 Effect of contact time on adsorption capacity of different dyes by PDA-Fe_3O_4. Experimental conditions: Initial dye (MB, JGB, MG, RhB, NR, CR, MO)=100 mg/L; adsorbents dosage=0.5 g/L; temperature=25℃±1℃.

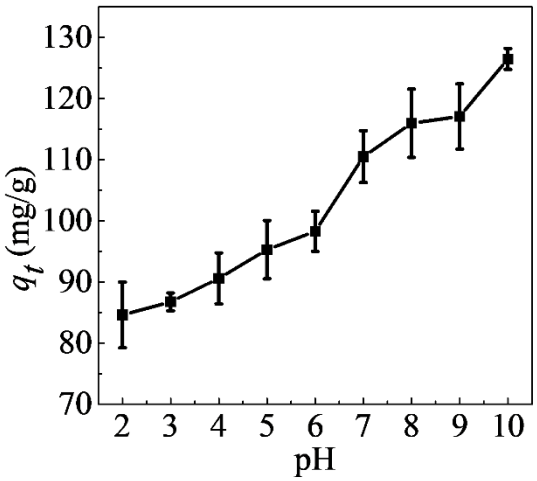

Fig. S5 Effects of initial pH on the adsorption of MB onto PDA-Fe_3O_4-Ag Experimental conditions: Initial dye (MB) =100 mg/L; adsorbents dosage=0.5 g/L; temperature=25℃±1℃.

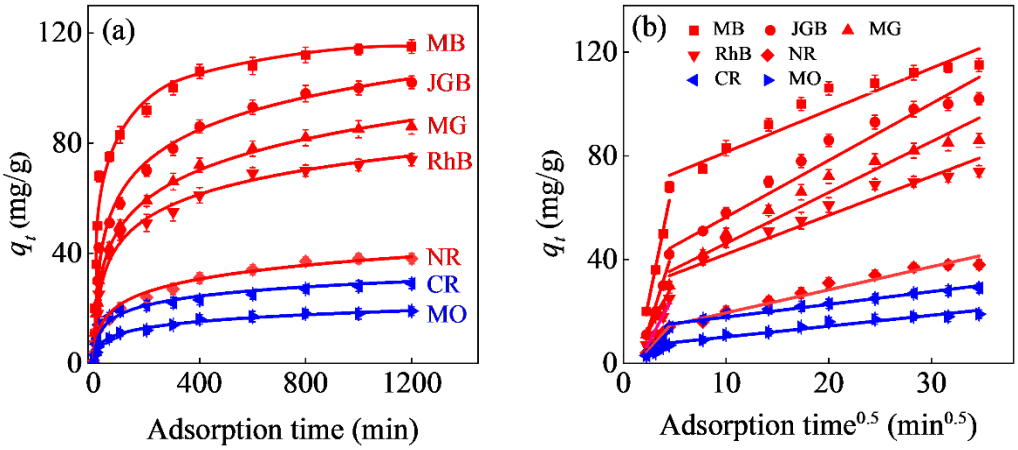

Fig. S6 Adsorption models for different dyes adsorption by PDA-Fe_3O_4-Ag: (a) Quasi-secondary model; (b) Intra-particle diffusion model.

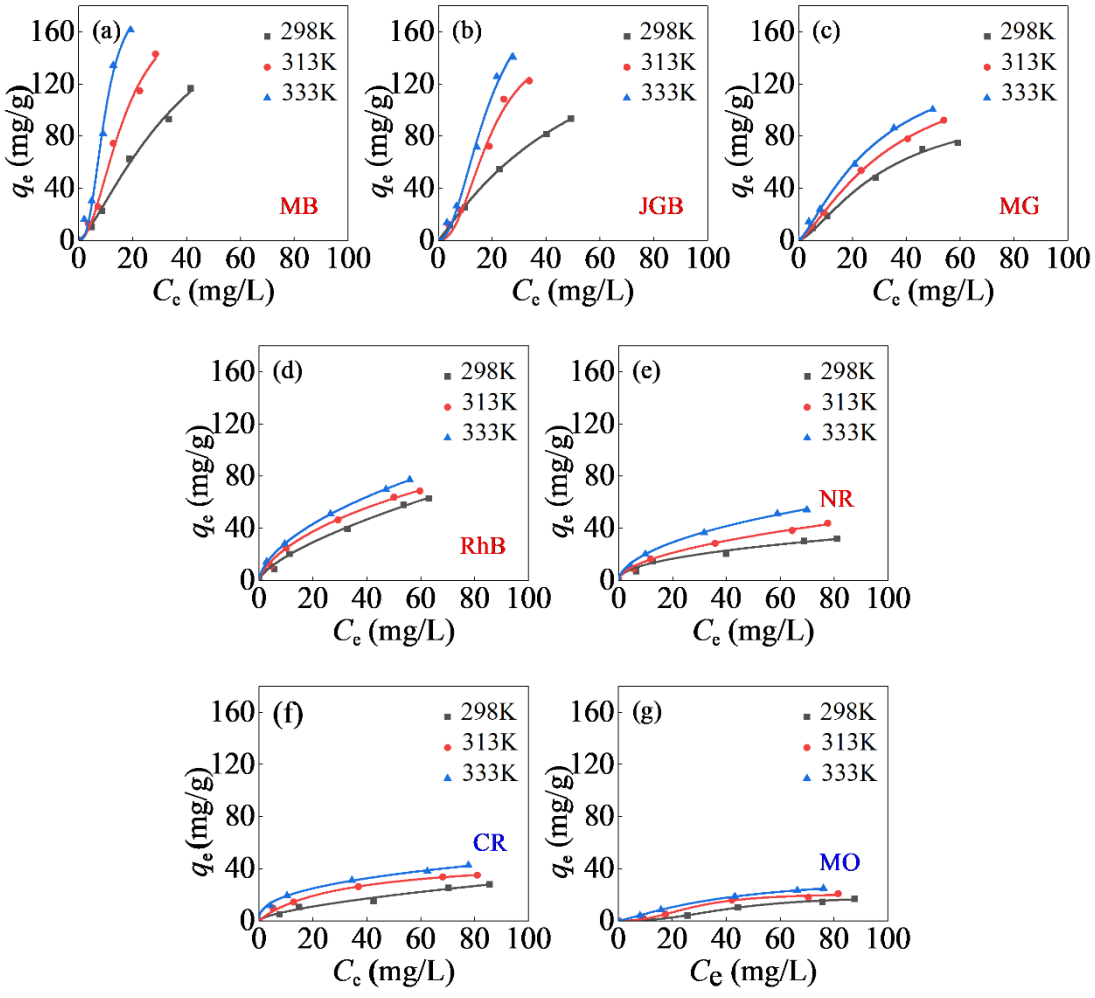

Fig. S7 Langumir isotherms of PDA-Fe_3O_4-Ag for different dyes adsorption: (a) MB, (b) JGB, (c) MG, (d) RhB, (e) NR, (f) CR, (g) MO.

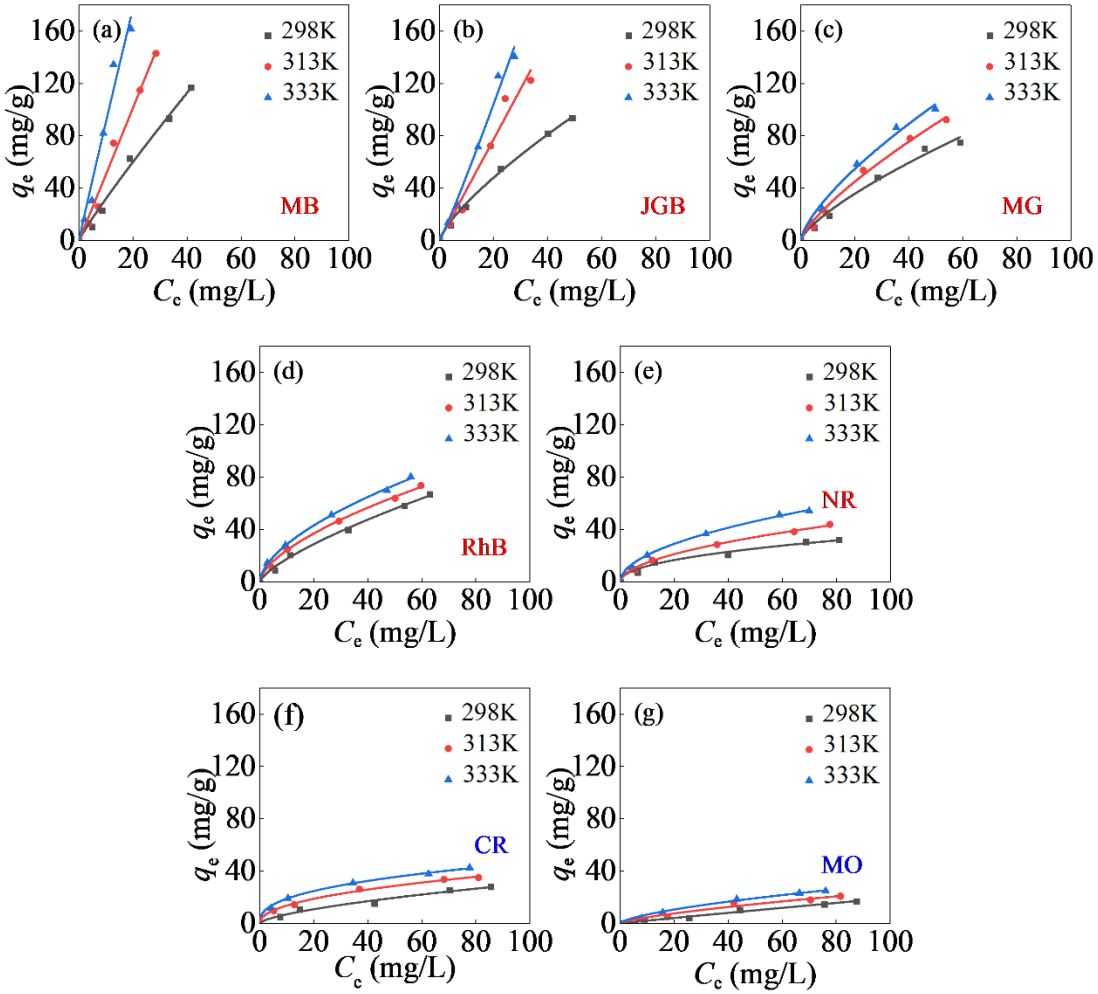

Fig. S8 Freundlich isotherms of PDA-Fe_3O_4-Ag for different dyes adsorption: (a) MB, (b) JGB, (c) MG, (d) RhB, (e) NR, (f) CR, (g) MO.

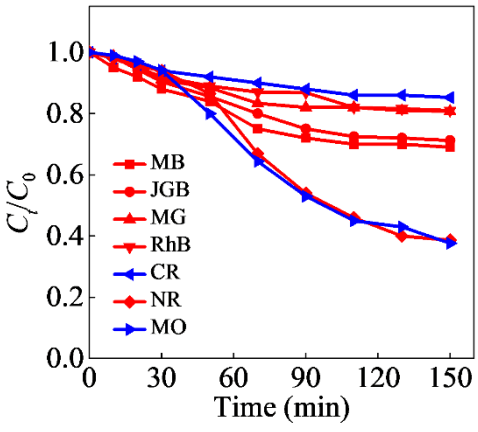

Fig. S9 Photocatalytic degradation behavior of PDA-Fe_3O_4-Ag. Experimental conditions: Initial dye (MB, JGB, MG, RhB, NR, CR, MO)=5 mg/L; catalysts dosage=1.25 g/L; temperature=25℃±1℃.

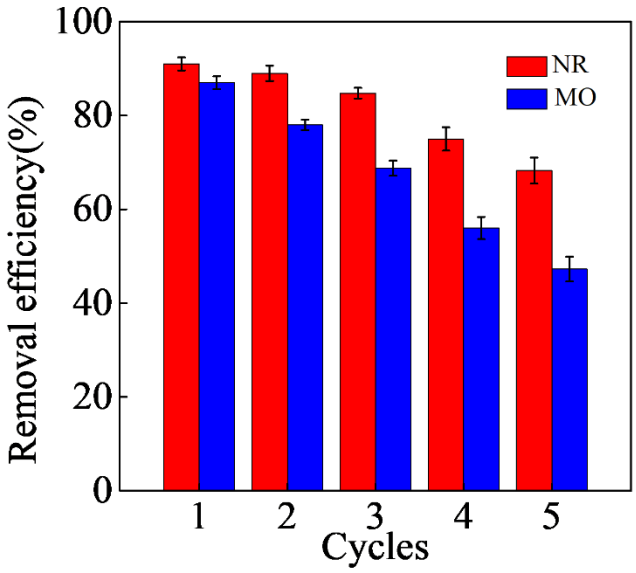

Fig. S10 Catalytic degragdation cycle of dyes NR and MO by PDA-Fe_3O_4-Ag. Experimental conditions: Initial dye (NR, MO)=5 mg/L; catalysts dosage=1.25 g/L; temperature=25℃±1℃.

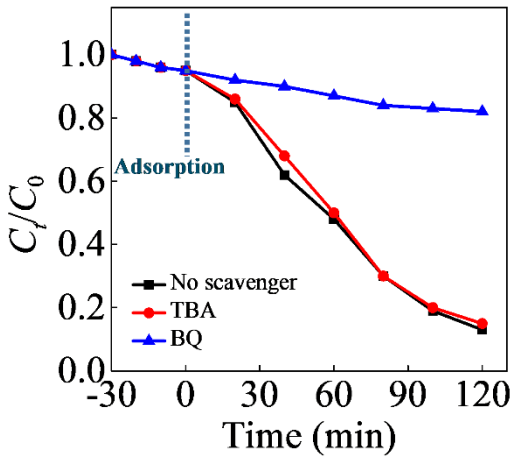

Fig. S11 Effects of radical scavengers on MO removal by PDA-Fe_3O_4-Ag. Experimental conditions: Initial MO=5 mg/L; catalysts dosage=1.25 g/L; scavengers=1 mmol/L; temperature=25℃±1℃.

Table S1 Comparison of the adsorption capacity of different adsorbents for MB dyes.

Adsorbents	q_{max} [a] (mg/g)	T (℃)	References
Silkworm exuviae	25.5	25	(Balakrishnan and Thiagarajan, 2021)
Zeolite/Fe_3O_4	32.3	25	(Wahyuni et al., 2021)
PDA[b]-rGO[c]-kaolin	39.6	25	(He et al., 2019)
PDA@DCA-COOH	69.9	25	(Chen et al., 2020)
PIL[d]@PDA@Fe_3O_4	72.5	25	(Lu et al., 2017)
DA[e]@PDA composite nanofiber membrane	88.2	25	(Cheng et al., 2020)
PDA microspheres	90.7	25	(Fu et al., 2015)
RHAC[f]	96.8	25	(Li et al., 2020)
GO-NMSZ[g]	100	25	(Yue et al., 2019)
S-CD/Fe_3O_4/GO-SH[h]	106	25	(Li et al., 2021b)
Cyclodextrin polymers	113	25	(Wang et al., 2020)
Activated carbon	136	25	(Do et al., 2021)
H-PDA-MCs[i]	191	25	(Feng et al., 2021)
PDA-Fe_3O_4-Ag	115	25	This work

Notes: a) maximum adsorption capacity; b) polydopamme; c) reduced graphene oxide; d) poly(ionic liquid); e) deacetylated cellulose acetate; f) Rice husk based activated carbon; g) Nano-silica/zinc/graphene oxide composite; h) Sulthydryl modified beta-cyclodextrin/Fe_3O_4/graphene oxide magnetic nanohybrid; i) hollow polydopamine microcapsules.

Table S2 Thermodynamic parameters of PDA-Fe_3O_4-Ag for different dyes adsorption.

Dyes	PDA-Fe_3O_4-Ag $\triangle G^0$ (KJ/mol)			$\triangle S^0$ (KJ/mol/K)	$\triangle H^0$ (KJ/mol)
	298K	313K	333K		
MB	–0.113	–0.796	–1.74	46.4	13.7
JGB	–0.277	–0.591	–0.811	15.2	4.23
MG	0.891	0.130	–0.633	43.5	13.8
RhB	0.719	–0.488	–1.01	49.0	15.2
NR	0.727	0.525	–0.573	37.4	12.0
CR	1.23	0.606	–1.31	158	50.7
MO	1.47	0.387	–2.82	–123	–38.3

Table S3 Comparison of the photocatalytic performance of different catalysts for MO.

Catalyst	Photocatalysis parameters	Catalytic activity	References
$BiVO_4$	10 mg/L MO dye 75 mg catalyst 500 W halogen lamp	Degradation=15.5% 60 min	(Srinivasan et al., 2022)
TiO_2/Ag_3VO_4/Gp [a)]	10 mg/L MO dye 20 mg catalyst 500 W visible light	Degradation=72.4% 240 min	(Motora et al., 2020)
ZnO-rGO	10 mg/L MO dye 50 mg catalyst 75 W visible light	Degradation=75.3% 180 min	(Ranjith et al., 2017)
NiO nanobelts	10 mg/L MO dye 60 mg catalyst 300 W visible light	Degradation=79.1% 140 min	(Kitchamsetti et al., 2021)
MWCNTs/TiO_2	20 mg/L MO dye 20 mg catalyst 400 W visible light	Degradation=80.0% 240 min	(Riaz et al., 2020)
PDA-Fe_3O_4-Ag	5 mg/L MO dye 50 mg catalyst 300 W visible light	Degradation=87.5% 120 min	This work

Notes: a) graphene.

Table S4 The degradation rate constants of blank and PDA-Fe_3O_4-Ag for different dyes.

Dyes	K (/min)	
	Blank	PDA-Fe_3O_4-Ag
MB	0.230×10^{-2}	0.230×10^{-2}
JGB	0	0.190×10^{-2}
MG	0	0.140×10^{-2}
RhB	0	0.110×10^{-2}
NR	0.0800×10^{-2}	2.11×10^{-2}
CR	0	0.0700×10^{-2}
MO	0	1.73×10^{-2}

Table S5 The binding energy and assignment of C 1s, N 1s and O 1s XPS spectral bands for PDA-Fe_3O_4-Ag and PDA-Fe_3O_4-Ag-MB.

Element	PDA-Fe_3O_4-Ag	PDA-Fe_3O_4-Ag-MB	Assignments
C 1s	284.14	283.97	C–C/C=C
	284.97	284.77	C–N
	286.04	285.43	C–O
	287.39	287.56	C=O
N 1s	399.43	399.45	–NH–
	400.07	400.21	$–NH_2$
O 1s	530.31	530.74	Fe–O
	532.08	532.41	C=O
	533.06	533.20	C–O

References

Alamin N U, Khan A S, Nasrullah A, Iqbal J, Ullah Z, Din I U, Muhammad N, Khan S Z (2021). Activated carbon-alginate beads impregnated with surfactant as sustainable adsorbent for efficient removal of methylene blue. International Journal of Biological Macromolecules, 176: 233–243

Balakrishnan J, Thiagarajan Y R (2021). Characterization and potential suitability of simarouba glauca seed shell lignocellulosic biomass as adsorbent of basic dyes from aqueous solutions. Cellulose Chemistry and Technology, 55(5–6): 705–722

Banisheykholeslami F, Hosseini M, Najafpour Darzi G (2021). Design of PAMAM grafted chitosan dendrimers biosorbent for removal of anionic dyes: Adsorption isotherms, kinetics and thermodynamics studies. International Journal of Biological Macromolecules, 177: 306–316

Chen W, Ma H, Xing B (2020). Electrospinning of multifunctional cellulose acetate membrane and its adsorption properties for ionic dyes. International Journal of Biological Macromolecules, 158: 1342–1351

Cheng J, Zhan C, Wu J, Cui Z, Si J, Wang Q, Peng X, Turng L S (2020). Highly efficient removal of methylene blue dye from an aqueous solution using cellulose acetate nanofibrous membranes modified by polydopamine. ACS Omega, 5(10): 5389–5400

Do T H, Nguyen V T, Dung N Q, Chu M N, Kiet D V, Ngan T T K, Tan L V (2021). Study on methylene blue adsorption of activated carbon made from Moringa oleifera leaf. Hyderabad, INDIA. Materials Today: Proceedings, 38: 3405–3413

Feng M L, Yu S C, Wu P C, Wang Z W, Liu S H, Fu J W (2021). Rapid, high-efficient and selective removal of cationic dyes from wastewater using hollow polydopamine microcapsules: Isotherm, kinetics, thermodynamics and mechanism. Applied Surface Science, 542: 148633

Fu J W, Chen Z H, Wang M H, Liu S J, Zhang J H, Zhang J N, Han R P, Xu Q (2015). Adsorption of methylene blue by a high-efficiency adsorbent (polydopamine microspheres): Kinetics, isotherm, thermodynamics and mechanism analysis. Chemical Engineering Journal, 259: 53–61

Giannakoudakis D A, Anastopoulos I, Barczak M, Antoniou E, Terpiłowski K, Mohammadi E, Shams M, Coy E, Bakandritsos A, Katsoyiannis I A, Colmenares J C, Pashalidis I (2021). Enhanced uranium removal from acidic wastewater by phosphonate-functionalized ordered mesoporous silica: Surface chemistry matters the most. Journal of Hazardous Materials, 413: 125279

He K, Zeng G M, Chen A W, Huang Z Z, Peng M, Huang T T, Chen G Q (2019). Graphene hybridized polydopamine-kaolin composite as effective adsorbent for methylene blue removal. Composites. Part B, Engineering, 161: 141–149

Kitchamsetti N, Ramteke M S, Rondiya S R, Mulani S R, Patil M S, Cross R W, Dzade N Y, Devan R S (2021). DFT and experimental investigations on the photocatalytic activities of NiO nanobelts for removal of organic pollutants. Journal of Alloys and Compounds, 855: 157337

Li P, Wang T, He J, Jiang J, Lei F (2021a). Synthesis, characterization, and selective dye adsorption by pH- and ion-sensitive polyelectrolyte galactomannan-based hydrogels. Carbohydrate Polymers, 264: 118009

Li X, Ma Y X, Shi X F, Kang X Y, Bai F M, Zhang D J (2021b). Sulfhydryl modified beta-cyclodextrin/Fe3O4/graphene oxide magnetic nanohybrid for the adsorption of silver ions and cationic dye methylene blue. Desalination and Water Treatment, 226: 419–430

Li Y, Pan B, Miao H Y, Xu H M, Liu X F, Shi G (2020). Single and binary dye adsorption of methylene blue and methyl orange in alcohol aqueous solution via rice husk based activated carbon: Kinetics and equilibrium studies. Chemical Research in Chinese Universities, 36(6): 1272–1278

Lu Y Y, Zhu H, Wang W J, Li B G, Zhu S P (2017). Collectable and recyclable mussel-inspired poly(ionic liquid)-based sorbents for ultrafast water treatment. ACS Sustainable Chemistry & Engineering, 5(4): 2829–2835

Motora K G, Wu C M, Xu T Z, Chala T F, Lai C C (2020). Photocatalytic, antibacterial, and deodorization activity of recycled triacetate cellulose nanocomposites. Materials Chemistry and Physics, 240: 122260

Ranjith K S, Manivel P, Rajendrakumar R T, Uyar T (2017). Multifunctional ZnO nanorod-reduced graphene oxide hybrids nanocomposites for effective water remediation: effective sunlight driven degradation of organic dyes and rapid heavy metal adsorption. Chemical Engineering Journal, 325: 588–600

Riaz A, Zhou C M, Xu J J, Hong Z L (2020). Photocatalytic performance of MWCNTs/TiO2 nanocomposites: conventional vs. microwave-assisted synthesis. Integrated Ferroelectrics, 211(1): 175–183

Srinivasan N, Anbuchezhiyan M, Harish S, Ponnusamy S (2022). Efficient catalytic activity of BiVO4 nanostructures by crystal facet regulation for environmental remediation. Chemosphere, 289: 133097 doi:10.1016/j.chemosphere.2021.133097

Wahyuni E T, Rendo D, Suherman S (2021). Removal of methylene blue dye in water by using recoverable natural zeolite/Fe3O4 adsorbent. Global NEST Journal, 23(1): 119–126

Wang J, Cheng G, Lu J, Chen H, Zhou Y (2020). PDA-cross-linked beta-cyclodextrin: a novel adsorbent for the removal of BPA and cationic dyes. Water Science and Technology, 81(11): 2337–2350

Wang W, Zhang X, Zhang Y H, Mi X, Wang R, Shi H L, Li C L, Du Z W, Qiao Y M (2021). Adsorption of emerging sodium p-perfluorous nonenoxybenzene sulfonate (OBS) onto soils: Kinetics, isotherms and mechanisms. Pedosphere, 31(4): 596–605

Yue Y, Cao Z, Yang F, Wang J, Abrahams I (2019). Preparation of an anti-aggregation silica/zinc/graphene oxide nanocomposite with enhanced adsorption capacity. Chemistry (Weinheim an der Bergstrasse, Germany), 25(71): 16340–16349 doi:10.1002/chem.201903875

Zhang T, Jin X, Owens G, Chen Z (2021). Remediation of malachite green in wastewater by ZIF-8@Fe/Ni nanoparticles based on adsorption and reduction. Journal of Colloid and Interface Science, 594: 398–408